Geophysical Research Letters

RESEARCH LETTER
10.1029/2020GL090963

Tropical Cyclone Integrated Kinetic Energy in an Ensemble of HighResMIP Simulations

Philip Kreussler[1,2], Louis-Philippe Caron[1], Simon Wild[1], Saskia Loosveldt Tomas[1], Fabrice Chauvin[3], Marie-Pierre Moine[4], Malcolm J. Roberts[5], Yohan Ruprich-Robert[1], Jon Seddon[5], Sophie Valcke[4], Benoît Vannière[6], and Pier Luigi Vidale[6]

[1]Barcelona Supercomputing Center (BSC), Barcelona, Spain, [2]GEOMAR – Helmholtz Centre for Ocean Research Kiel, Kiel, Germany, [3]Centre National de Recherches Météorologiques, Université de Toulouse, CNRS, Météo-France, Toulouse, France, [4]CECI, Université de Toulouse, CNRS, CERFACS, Toulouse, France, [5]Met Office, Exeter, UK, [6]National Centre for Atmospheric Science (NCAS), University of Reading, Reading, UK

Abstract This study investigates tropical cyclone integrated kinetic energy, a measure which takes into account the intensity and the size of the storms and which is closely associated with their damage potential, in three different global climate models integrated following the HighResMIP protocol. In particular, the impact of horizontal resolution and of the ocean coupling are assessed. We find that, while the increase in resolution results in smaller and more intense storms, the integrated kinetic energy of individual cyclones remains relatively similar between the two configurations. On the other hand, atmosphere-ocean coupling tends to reduce the size and the intensity of the storms, resulting in lower integrated kinetic energy in that configuration. Comparing cyclone integrated kinetic energy between a present and a future scenario did not reveal significant differences between the two periods.

Plain Language Summary The damage potential of tropical cyclones is often described by their maximum wind speed. However, maximum wind speed is not particularly well correlated with tropical cyclone losses because intensity defined in such a way does not take into account the size of the storm, which is an important factor driving tropical cyclone related losses. Tropical cyclone integrated kinetic energy on the other hand is a measure which takes into account both the size and the intensity of the cyclones and is more representative of its destructiveness. Here, we investigate integrated kinetic energy in three different global climate models following a common protocol. We find that an increase in horizontal model resolution results in smaller and more intense storms, but that the range of integrated kinetic energy produced by the models remains similar in both configurations. On the other hand, allowing the atmosphere and ocean to interact with each other in the models tends to reduce the size and the intensity of the storms, resulting in lower integrated kinetic energy. Comparing cyclone integrated kinetic energy between present conditions and a projected future climate scenario did not suggest notable changes between the two periods.

Key Points:

- Increasing horizontal resolution leads to smaller and more intense tropical cyclones but relatively similar integrated kinetic energy
- Coupling atmosphere and ocean tends to reduce the size and intensity of cyclones, generally resulting in lower integrated kinetic energy
- Comparing integrated kinetic energy between present and projected future conditions does not reveal significant differences between the two

Supporting Information:

- Supporting Information S1

Correspondence to:
P. Kreussler,
philip.kreussler@bsc.es

Citation:
Kreussler, P., Caron, L.-P., Wild, S., Loosveldt Tomas, S., Chauvin, F., Moine, M.-P., et al. (2021). Tropical cyclone integrated kinetic energy in an ensemble of HighResMIP simulations. *Geophysical Research Letters*, *48*, e2020GL090963. https://doi.org/10.1029/2020GL090963

Received 28 SEP 2020
Accepted 12 FEB 2021

1. Introduction

Tropical cyclones (TCs) are one of the costliest natural catastrophes (A. Benfield, 2018; Emanuel, 2005; Landsea, 2000) as they can bring a number of hazards such as high winds, heavy precipitation, storm surges, inland and coastal flooding, tornadoes, and landslides. *Hurricane Katrina* (2005) is currently the costliest TC on record with US$160 billion in damage (National Hurricane Center, 2018), but other recent examples such as *Hurricane Dorian* (2019) and *Cyclone Harold* (2020), which caused widespread damage across the Bahamas and the South Pacific respectively, have shown that TCs also have the potential to threaten some of the most vulnerable countries to devastating effect.

Traditionally, the destructive potential of TCs has been estimated using the near surface 1-min maximum sustained wind speed and their corresponding classification on the Saffir-Simpson Scale (Simpson, 1971). However, such classification is not always representative of the damage a storm can cause because it neglects an important component of the storm: its size. A number of studies have emphasized the benefits of considering the size and structure of the storm when estimating TC-related damage (Kantha, 2006; Mahendran, 1998; Wang & Toumi, 2018a; Zhai & Jiang, 2014). In fact, the past 2 decades have also provided

clear examples of this: *Ivan* (2004), *Katrina* (2005), and *Sandy* (2012) were not particularly high on the Saffir-Simpson scale at landfall, yet caused extensive damage. For Hurricane *Ivan* and *Sandy* in particular, the damage can be explained by the continuous expansion of the storm in the mature stage (Wang & Toumi, 2018a).

To address this shortcoming, the so-called Integrated Kinetic Energy (IKE; Powell & Reinhold, 2007) metric was developed. This metric takes the size of the storm into account by integrating the energy over the entire wind field of the storm. With this metric, the aforementioned storms rate as significantly more dangerous than on the Saffir-Simpson scale owing to the large extent of their wind fields at landfall, which is more in line with the large devastation they brought (Kantha, 2006; Kozar & Misra, 2019; Powell & Reinhold, 2007).

With a typical diameter of a few hundred kms (Chavas & Emanuel, 2010), TCs are (relatively) small-scale phenomena which cannot be entirely resolved by CMIP-type global climate models. In fact, TC activity is notoriously difficult to reproduce in certain basins and the importance of increasing horizontal model resolution to address this issue has long been recognized (Bengtsson et al., 2007; Camargo, 2013; Camargo & Wing, 2016; Moon et al., 2020; Caron et al., 2011; Roberts et al., 2015; Strachan et al., 2013; Wehner et al., 2015). It is thought that horizontal resolution will address other long standing issues as well, such as more realistic TC wind speeds and size. As such, many different technical solutions have been attempted, from dynamical downscaling (Caron & Jones, 2012; Lavender & Walsh, 2011; Patricola et al., 2018), to global-variable resolution models (Caron et al., 2013; Daloz et al., 2012; Zarzycki & Jablonowski, 2014) to statistical-dynamical downscaling through random seeding (Baudouin et al., 2019; Emanuel, 2013; Lee et al., 2018).

Here, we investigate how IKE, which has been relatively unexplored in climate models compared to other TC characteristics, is represented in a series of global climate models and how it is impacted by the horizontal resolution and the coupling of the atmosphere model to the ocean model. The impact of the resolution is investigated using a brute-force approach, wherein the global climate models are all run at both a standard and a higher resolution following a strict protocol. The structure of this study is as follows: Section 2 provides an overview of the experimental setup and the cyclone tracker, while the impacts of resolution, coupling and change in atmospheric forcings are investigated in Section 3. A brief conclusion is provided in Section 4.

2. Models, Data, and Experimental Setup

This study is carried out using data produced within the European PRIMAVERA project (Roberts et al., 2018) as a part of the CMIP6 High Resolution Model Intercomparison Project (HighResMIP; Haarsma et al., 2016). HighResMIP provides a protocol for investigating the impact of horizontal resolutions on climate simulations and as such, requires all model configurations to be the same for both resolutions so that differences can directly be attributed to the change in resolution rather than to model physics or adjustments of parameterizations. The experiments evaluated here are performed at two different model resolutions, a standard/lower resolution (LR) and a higher resolution (HR), and each model configuration was run in both an atmosphere-only mode using prescribed ocean and sea ice conditions and in coupled mode. Each configuration covers a historical period (1950–2014) which uses observed atmospheric forcings (present) and a future projection (2015–2050) which uses forcings derived from the SSP5-8.5 scenario (future). In each simulation, we track the storms between 0° and 40°N in both the Northern Pacific and Northern Atlantic (for convenience referred to as Northern Hemisphere [NH]) basins from June to November.

Here, we use three global climate models (GCMs), ranging in nominal atmospheric resolution from 250–100 km in LR to 50 km in HR: CNRM-CM6-1 (Voldoire et al., 2019), EC-Earth3P (Haarsma et al., 2020), and HadGEM3-GC31 (Roberts et al., 2019). The 6-h model output used is available on the Earth System Grid Federation nodes under references: CNRM-CM6-1 (Voldoire, 2019a, 2019b), EC-Earth3P (EC-Earth, 2018; EC-Earth, 2019), and HadGEM3-GC31 (Roberts, 2017a, 2017b). A brief overview of the tracking algorithm and model resolutions used to carry out these experiments are provided in the supporting information (Text S1) and Table S1.

2.1. Tropical Cyclone Tracker

The cyclone tracker used to detect the formation and propagation of TCs is the Geophysical Fluid Dynamics Laboratory Vortex Tracker V3.5b (Biswas et al., 2018) which we implemented in ESMValTool (Eyring et al., 2019; Righi et al., 2020). Information on the variables required by the tracker and the tracking process can be found in Text S1. The advantage of using this cyclone tracker is the direct output of IKE by the tracker. Unlike other integrated measures like the Accumulated Cyclone Energy index (ACE; Bell et al., 2000), IKE takes into account the entire wind field at any given time step. IKE is defined as the volume integral of the kinetic energy $KE = \frac{\rho U^2}{2}$ per volume unit of the horizontal wind field of a storm over a uniform 1-m slice, centered at 10 m height with a spatially uniform air density $\rho = 1\ kgm^{-3}$:

$$IKE = \int_V KE\ dV = \int_V \frac{\rho U^2}{2}\ dV = \frac{1}{2}\ kg\ m^{-2} \cdot \int_A U^2\ dA \tag{1}$$

All grid points with wind speeds larger than 18 ms^{-1} (threshold for tropical storms) are used to compute the storms' IKE. Reducing the threshold to 10 ms^{-1} increases IKE but did not significantly impact the results. Also, only grid points within a 2,000-km square around the storm center are considered for the computation of the IKE. An example of an area considered in the computation of IKE is provided in Figure S1. We also integrated the IKE of each storm over their entire lifetime and summed up each storm's total IKE during that season. Henceforth referred to as the seasonally accumulated IKE, this metric reflects integrated TC characteristics, such as numbers, duration, and time at maximum intensity. Finally, the lifetime maximum IKE of observed TCs is estimated using the λ model described in Wang and Toumi (2016) using data from IBTrACS (Knapp et al., 2018) for storms located between 0° and 40°N for which information on the size of the storm was available.

3. Results

We first provide an overview of the GCMs' ability to represent TCs in the NH. Figure 1 shows all TCs generated in the models over a 30-year period. For all three models, it is obvious that increasing resolution leads to more storms, which is consistent with previous studies (Caron et al., 2011; Manganello et al., 2012; Roberts et al., 2015, 2020a, 2020b). The Western North Pacific basin (WNP) is the basin that sees the largest increase in absolute numbers, but the Eastern North Pacific (ENP) and the North Atlantic (NA) basins see the largest increase in relative terms due to the fact that generally few storms form in these basins in LR. In particular, the ENP is biased extremely low in all LR experiments with respect to observations (Ramsay, 2017) and almost all model configurations strongly underestimate the hurricane frequency in the main development region (MDR; Goldenberg & Shapiro, 1996) over the Atlantic. In fact, none of the LR simulations display what could be referred to as a MDR over the tropical Atlantic. Historically, simulating realistic TC activity in both these basins has proven particularly challenging for climate models (Camargo, 2013; Camargo et al., 2016). Overall, only the HadGEM3-GC31 HR configurations are able to produce mean annual storm counts close to observations (WNP: 25, ENP: 15, NA: 13; Ramsay, 2017) while the remaining HadGEM3-GC31 configurations and all EC-Earth3P and CNRM-CM6-1 configurations are biased low with respect to observations. We note that using a resolution-dependent intensity threshold for TC detection as suggested by Walsh et al. (2007) also leads to higher TC numbers in HR compared to LR in all configurations (Figure S2), so this gap in TC activity between the two sets of simulations is not the product of the tracking algorithm but represents a genuine difference in TC formation in HR compared to LR.

In general, the coupled experiments show fewer storms than the atmosphere-only experiments, although there are some notable exceptions such as the ENP in EC-Earth3P and CNRM-CM6-1 at high resolution. Furthermore, the coupled experiments show storms that are less intense than atmosphere-only experiments, likely due to the ocean feedback on the storm systems (Cione & Uhlhorn, 2003; Emanuel, 2001) and the CNRM-CM6-1 HR atmosphere-only experiment is the only integration which generates TCs of category 3 or higher on the Saffir-Simpson scale (Figure 1c) and thus represents wind speeds closer to observations than the other integrations. This feature of the CNRM-CM6-1 model has been highlighted before (Roberts

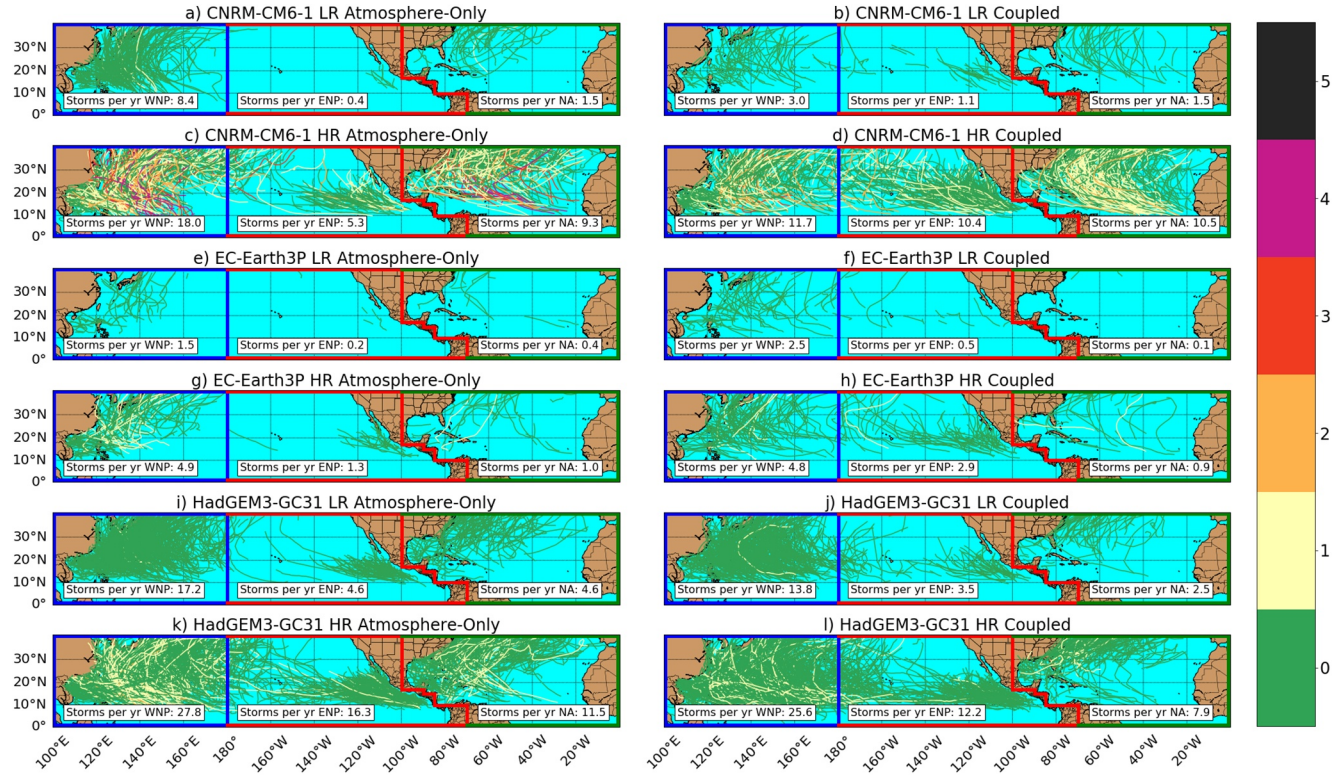

Figure 1. Tropical cyclone tracks for the CNRM-CM6-1, EC-Earth3P, and HadGEM3-GC31 models, for both atmosphere-only and coupled configurations and at both standard and high resolution. The period considered is 1950–1980. The color represents the maximum intensity of the storms, as measured by the Saffir-Simpson scale.

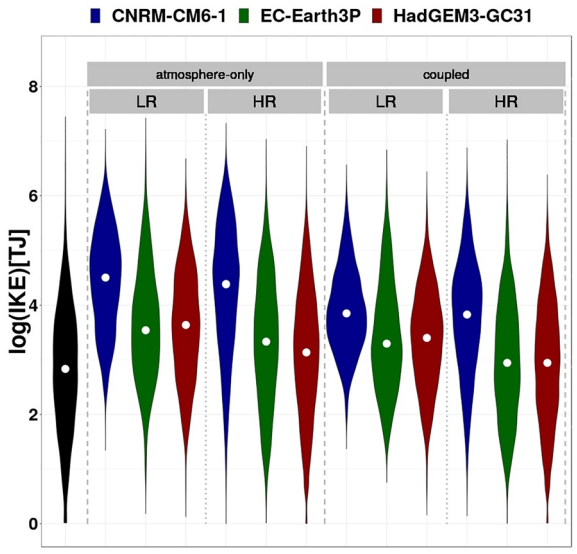

Figure 2. Distribution of lifetime maximum IKE in the NH for each climate model configuration and for a reference observation-based model (black). The reference is based on the λ model developed by Wang and Toumi (2016) and uses data for which information on the size of TCs is available in IBTrACS (2001–2020). White dot indicates median of distribution. Note that the *y*-axis is on a log-scale. IKE, Integrated Kinetic Energy; NH, Northern Hemisphere; TC, Tropical cyclone.

et al., 2020a) and seems to be linked to a newly implemented turbulence scheme (Hersbach et al., 2020). Overall, these results are consistent with the results of Roberts et al. (2020a, 2020b) obtained using different tracking algorithms.

Having established the general TC climatology of the different model configurations, we can now compare the IKE of the TCs in these simulations. Figure 2 shows the distribution of lifetime maximum IKE in each model configuration (and for each basin individually in Figures S3–S5). Most models tend to overestimate IKE, with EC-Earth3P HR and HadGEM3-GC31 HR in coupled mode producing IKE that are closest to the reference data set. The CNRM-CM6-1 model in particular produces storms with considerably higher IKE than the other two models, regardless of the configuration. We also notice that coupling tends to reduce IKE. Perhaps surprisingly, maximum IKE values for a given model show a comparable range in LR and HR in all cases, which stands in strong contrast to maximum surface winds and the intensity measured by the Saffir-Simpson scale (Figure 1).

However, it is obvious from Figure 3 that LR and HR achieve similar IKE values for different reasons: TCs in LR tend to be larger, but weaker, than TCs in HR. This is made clear by the different regression lines computed using only TCs in LR (full lines) or HR (dashed lines): These lines show that in all models and configurations, HR generally produces smaller storms for a given wind speed. The CNRM-CM6-1 model in particular produces storms with considerably higher IKE than the other two

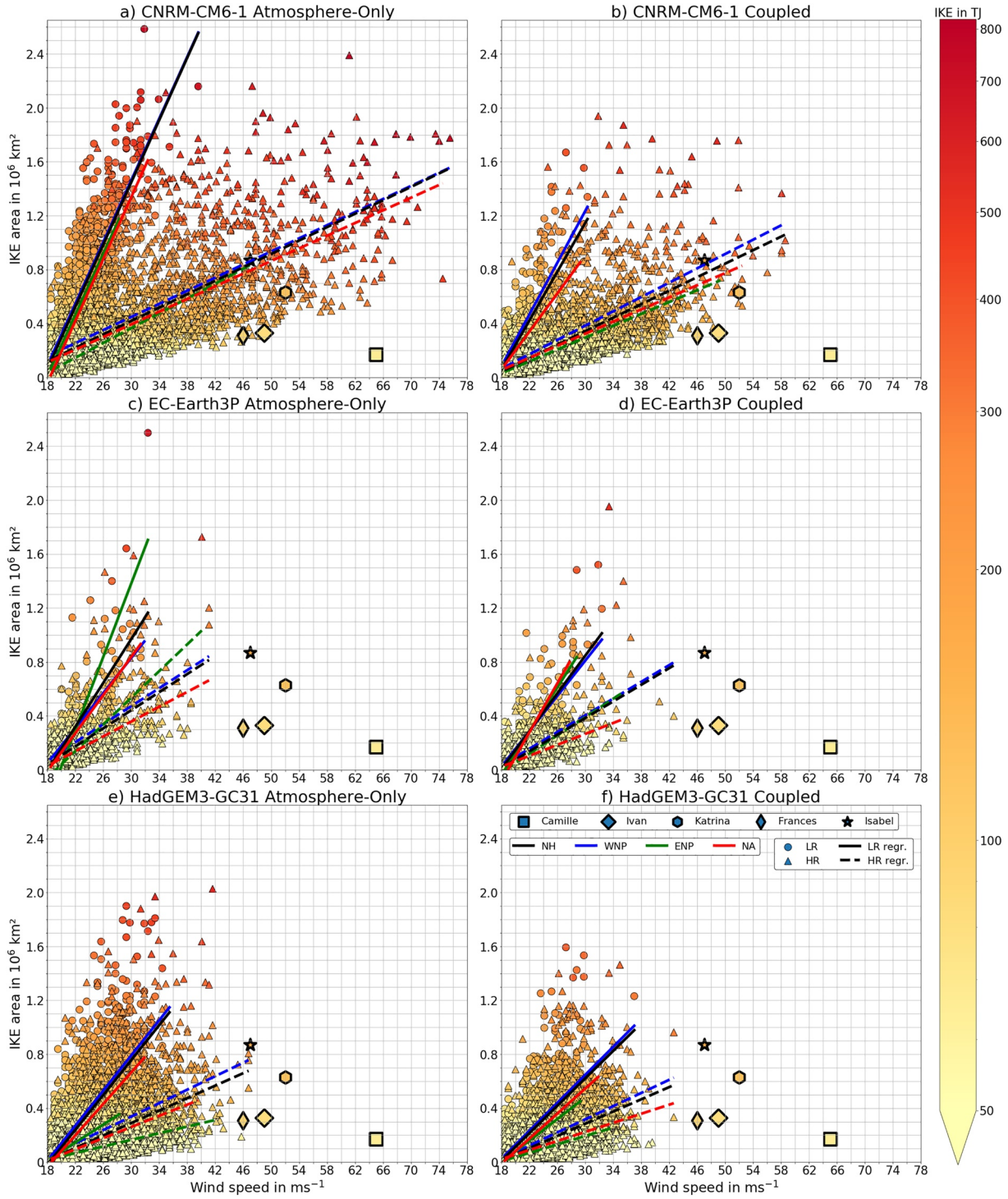

Figure 3. Scatterplots showing the TC lifetime maximum IKE (color) as well as the corresponding maximum surface wind and the area contributing to the IKE for the CNRM-CM6-1 model (first row), EC-Earth3P (second row), and HadGEM3-GC31 (third row). Each circle (triangle) represents a storm at LR (HR). The atmosphere-only (coupled) experiments are in the left (right) column. The solid and dashed lines are regression lines for LR and HR, respectively. Linear regressions for storms in the NH are shown in black, WNP in blue, ENP in green, and NA in red. The period covered is 1950–2050. Observed historical storms are displayed with bigger markers and taken from Powell and Reinhold (2007). The size of the tropical storm wind field for observed storms in Powell and Reinhold (2007) is approximated by using the radius of the maximum wind speed R_{max} and the radius of the outer threshold of tropical storm strength R_{18}, assuming an axis-symmetric cylindrical storm and wind speeds below tropical storm strength at radii below R_{max}. ENP, Eastern North Pacific; HR, higher resolution; IKE, Integrated Kinetic Energy; LR, lower resolution; NA, North Atlantic; NH, Northern Hemisphere; TC, Tropical cyclone; WNP, Western North Pacific.

models due to the fact that the storms are both larger and their surface winds are much stronger than either EC-Earth3P or HadGEM3-GC31, particularly at high resolution: The latter seem to reach their maximum intensity at approximately 42 ms^{-1} while the former can reach values up to 76 ms^{-1}. While this impact of resolution on simulated TCs has been highlighted before, what is interesting to note here is that this has relatively little impact on the simulated IKE of the storms themselves. In other words, the increase in intensity with resolution tends to compensate for the decrease in size such that IKE remains relatively similar across resolutions.

Figure 3 also shows how simulated cyclones compare with five different notable Atlantic hurricanes at landfall (Powell & Reinhold, 2007). Only the CNRM-CM6-1 model at high resolution manages to produce storms similar to four of the five storms selected here (larger storms like *Hurricane Isabel* [2003] and *Hurricane Katrina* [2005] are relatively common in that model), but the model generally overestimates IKE at both LR and HR (consistent with findings from Figure 2) since the storms are much larger than what is typically observed. Smaller storms with similar intensity such as *Hurricane Frances* (2004) and *Hurricane Ivan* (2004) appear at the limit of what the model can produce while small intense storms like *Hurricane Camille* (1969) are beyond the capability of this model. And generally, the storms produced in EC-Earth3P and HadGEM3-GC31 bear little resemblance to observed storms, except possibly for the latter at HR in atmosphere-only mode.

We also note differences between the individual basins. The overall TC distributions for the NH (black line) generally follow the WNP (blue line), due to the larger number of storms occurring in that basin compared to the other two. Atlantic hurricanes are generally smaller in size than typhoons, which aligns with observations (Chavas & Emanuel, 2010). Finally, TCs simulated over the ENP are generally the smallest, especially in HadGEM3-GM31. This behavior is less evident in EC-Earth3P, however, possibly because of the low number of storms generated over that basin in that model. The coupled and atmosphere-only configurations generally have similar behavior: The difference between the two is mainly limited to the range of the maximum wind speed and maximum storm size. Figure S6 shows a shift in probability densities to smaller and less intense storms in the CNRM-CM6-1 and HadGEM3-GC31 models. This shift toward smaller and weaker storms is particularly obvious for the strongest cyclones, likely a result of the ocean feedback which limits the intensification of the cyclones (Figure S7).

Having compared IKE in the different configurations, we will now try to understand some of the differences that were detected, and more broadly what modulates IKE in these configurations. Correlations between lifetime maximum IKE and (i) the size of the storm and (ii) the maximum wind speed near the surface clearly show that the storm size is the dominant factor modulating IKE in all configurations (triangles, Figure S8), which is consistent with results from Wang and Toumi (2018a). It is interesting to note that there is a tendency for the minimum in mean sea level pressure (MSLP) to be a better predictor of IKE than maximum surface wind speed (orange squares vs. orange circles along the *y*-axis) at HR. While some of the differences in correlation between IKE-MSLP and IKE-wind are small, they are present in all configurations, something that is not observed at standard resolution (same symbols, *x*-axis). To understand why that might be, we performed the same analysis by dividing our data into two samples along the median in IKE. The red symbols show the same correlations for storms in the upper part of the distribution. We note that the correlations with respect to MSLP and maximum wind speed are generally lower, but the differences between the two have increased, which suggest that this discrepancy is partly due to the inability of high-resolution climate models to capture the observed relationship between the minimum in MSLP and the maximum surface wind speeds. This is also supported by the fact that the correlations with wind speed are higher in the CNRM-CM6-1 model, for which the wind-pressure relationship follows more closely the observations (Roberts et al., 2020a). Part of the reason for this difference could also come from the fact that the central pressure deficit is more closely tied to the size of the storm than the maximum in surface wind (Chavas et al., 2017).

3.1. Projected Activity

We conclude our analysis by evaluating whether there is a change in IKE between present and future conditions in each of our coupled simulations. Recent studies using climate models suggest that certain TC characteristics, including precipitation or the lifetime maximum intensity, are projected to increase (Knutson

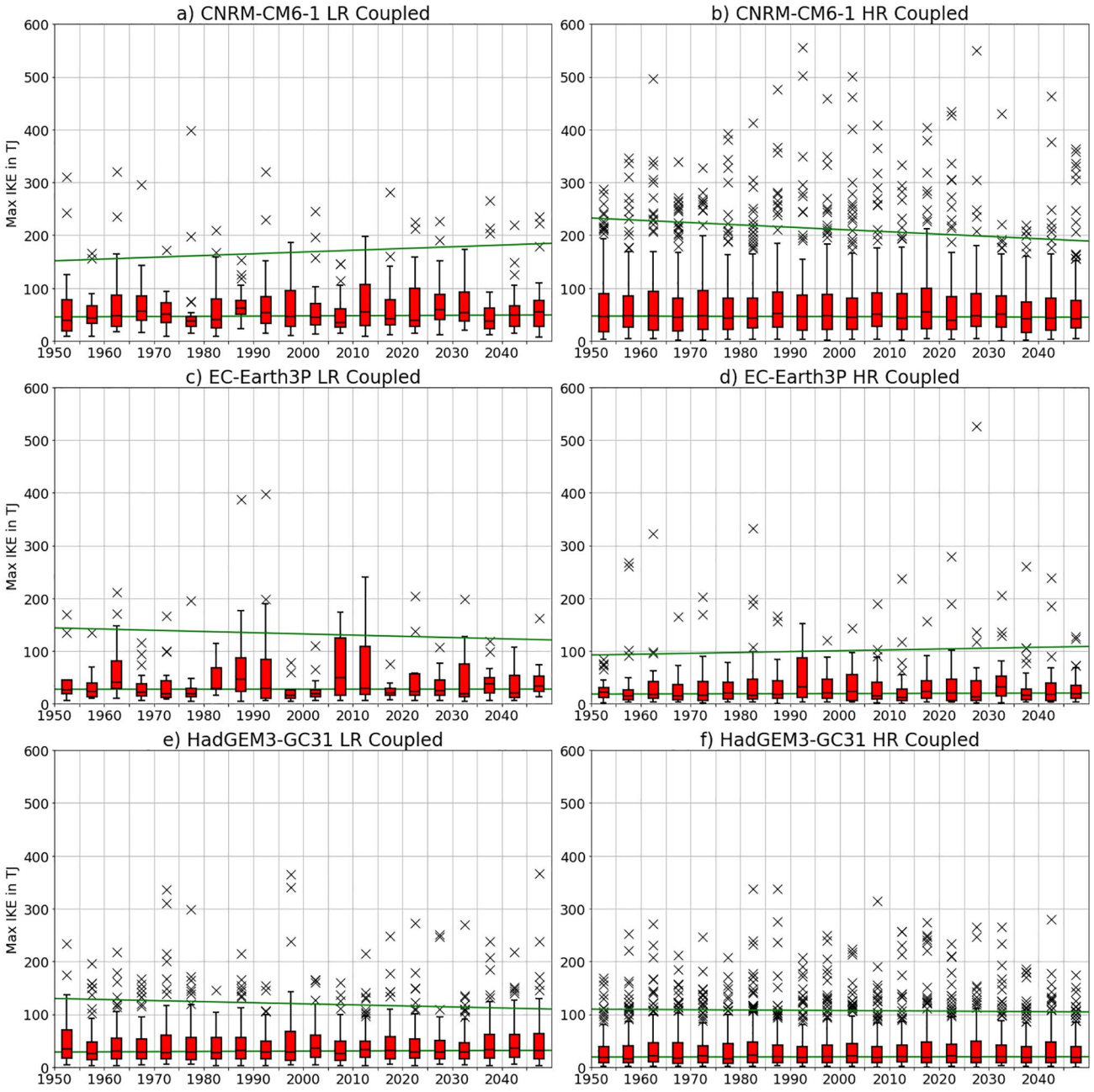

Figure 4. Boxplot of lifetime maximum IKE for storms in the NH for coupled integrations of CNRM-CM6-1 (top row), EC-Earth3P (second row) and HadGEM3-GC31 (bottom row) at LR (left column) and HR (right column). Each box represents a 5-year period. Trend lines (green) are shown for the median and the 95th percentile. The statistical significance of the trend in the 95th percentile is provided in Table S2. HR, higher resolution; IKE, Integrated Kinetic Energy; LR, lower resolution; NH, Northern Hemisphere.

et al., 2019). Projections of storm size are more scarce and uncertain, however, while some studies detected an increase in the size of TCs globally in a future climate (Emanuel, 2020; Kim et al., 2014; Yamada et al., 2017), other studies did not (Gutmann et al., 2018; Knutson et al., 2015; Wang & Toumi, 2018b).

Figure 4 shows the distribution of lifetime maximum IKE for the 1950–2050 period for each of the three models. While we detect some multi-annual variability, we do not detect a significant increase in the median IKE. Because most of the damage comes from the strongest storms and, as with changes in the surface wind, extremes are where we might expect to detect a change (Elsner et al., 2008; Elsner, 2020). This is because the strongest storms are the most likely to have reached or be near their maximum potential intensity,

which is controlled by the thermodynamic of the ocean-atmosphere system, which itself is sensitive to the change in radiative forcings. Thus, we also evaluated the trends for storms in the 95th percentile of each 5-year period and again found no significant trends in any of the simulations (based on a Mann-Kendall test whose null hypothesis is no trend, at the 5% level). In order to evaluate whether the absence of trends in maximum IKE was due to compensating trends in intensity and size, we also evaluated the trends in the TC area used to compute the IKE. No such trend was detected (Figure S9). This result is consistent with Roberts et al. (2020b), who detected only a weak increase in the intensity of TCs in PRIMAVERA simulations. Comparing probability distributions in lifetime maximum IKE between the 1950–1980 and 2020–2050 periods does not reveal any significant differences between the two time periods either (not shown), thus indicating that anthropogenic climate change did not have a detectable impact on IKE in our simulations.

We also evaluated the change in the mean seasonally accumulated IKE between the 1950–1980 and 2020–2050 periods, globally and for each of the three basins individually. While the responses would tend to suggest an increase (Figure S10), we note that only HadGEM3-GC31 LR over the NA and EC-Earth3P HR over the WNP and the NH as a whole show a statistically significant increase over the two periods (Table S3). It is also worth noting that besides EC-Earth3P in the ENP and NA where TC activity is poorly simulated to begin with, only the CNRM-CM6-1 model suggests a decrease in mean seasonally accumulated IKE and only does so in one basin.

Given that only TCs that come near land impact human activities, we repeated this latest analysis by considering only storms in the western part of the Pacific and Atlantic (i.e., storms that tracked west of 140°E in the Pacific and west of 60°W in the Atlantic). The results generally suggest an increase in TIKE (Figure S11), similar to what we obtained when we considered the entire basin, although most of the changes are not significant. The only simulations with a significant change in this case are HadGEM3-GC31 LR (increase) and CNRM-CM6-1 HR (decrease) over the North Atlantic.

4. Summary and Discussion

This study has investigated the impact of an increase in horizontal resolution on the representation of tropical cyclones in different climate models, with a special focus on IKE, a measure closely associated with the damage potential of TCs. For all three models and in both configurations, we found that an enhancement of the resolution leads to an increase in wind speed (Figures 1 and 3) and a decrease in storm size (Figure 3). These changes combine such that the range in lifetime maximum IKE remains relatively similar across resolutions, except for the most intense storms produced by CNRM-CM6-1 in HR. This result may be somewhat unexpected but aligns with the study by Vannière et al. (2020). TCs derive their kinetic energy from latent heat release during the ascent of moist air in the tropical cyclone and Vannière et al. (2020) showed that the distribution of precipitation averaged over the entire TC had little sensitivity to resolution for a given model. Taken in combination, these results suggest that the thermodynamic efficiency of TCs is not affected by resolution.

Analyses have shown that the storm size is the leading factor modulating IKE for all models and configurations. Interestingly, minimum in MSLP seems to be a better predictor of IKE in HR than the maximum wind speed, which tends to support the use of central pressure deficit as a better proxy than maximum surface winds to estimate TC damage (Klotzbach et al., 2020), even in climate simulations. Furthermore, our simulations show no significant changes in lifetime maximum IKE between present climate conditions and a projected climate scenario, which stands in contrast with previous studies. While we do not show it here, this result also applies to atmosphere-only simulations. It's worth noting that Roberts et al. (2020b) found that surface wind speed of TCs in PRIMAVERA simulations (including the models used here) projected an increase in TC intensity much below that of other modeling studies, which is somewhat consistent with the results obtained here. It is not yet clear why TCs in PRIMAVERA models appear less sensitive to an increase in forcings compared to that of other models.

Finally, it is important to point out that even though the IKE of individual storms is similar across resolutions, the mean seasonally accumulated IKE is much higher at HR simply because the number of storms is significantly larger in these simulations. And while IKE appears relatively insensitive to the range of resolution covered here, it would be interesting to check whether this holds true for models with even higher

resolution (say a few km range). We hope that integrating the tracker in the ESMValTool environment will provide the opportunity to other groups who have access to such simulations to investigate this issue, and, more generally, that this will facilitate the analysis of TCs in climate models.

Data Availability Statement

The data sets used in this work are cited with appropriate DOIs in publicly available archives. The 6-h model output used is available on the Earth System Grid Federation nodes (https://esgf-index1.ceda.ac.uk/search/cmip6-ceda) under references Roberts (2017a, 2017b), EC-Earth (2018); EC-Earth (2019) and Voldoire (2019a, 2019b). The IBTrACS data is provided by Knapp et al. (2018) and available under https://doi.org/10.25921/82ty-9e16.

Acknowledgments
This research has been supported by the Horizon 2020 programme (PRIMAVERA, GA #641727). S. Wild received funding from the European Union Horizon 2020 research and innovation programme under the Marie Sklodowska-Curie grant agreement 2020-MS-CA-COFUND-2016-754433 and financial support from the Spanish Agencia Estatal de Investigación (FJC2019-041186-I/AEI/10.13039/501100011033). M. J. Roberts acknowledges the support from the UK-China Research and Innovation Partnership Fund through the Met Office Climate Science for Service Partnership (CSSP) China as part of the Newton Fund. Finally, the authors are most grateful to three anonymous reviewers for their helpful comments in improving a previous version of this manuscript.

References

Baudouin, J. P., Caron, L. P., & Boudreault, M. (2019). Impact of reanalysis boundary conditions on downscaled Atlantic hurricane activity. *Climate Dynamics*, *52*(5–6), 3709–3727. https://doi.org/10.1007/s00382-018-4352-7. Retrieved from http://dx.doi.org/10.1007/s00382-018-4352-7

Bell, G. D., Halpert, M. S., Schnell, R. C., Higgins, R. W., Lawrimore, J., Kousky, V. E., et al. (2000). Climate assessment for 1999 Table of contents. *Bulletin of the American Meteorological Society*, *81*(6), 1–50.

Benfield, A. (2018). *Weather, climate & catastrophe insight2017 annual report. Aon Benfield UCL hazard research center report, 2–5*. Retrieved from http://thoughtleadership.aonbenfield.com/Documents/20180124-ab-if-annual-report-weather-climate-2017.pdf

Bengtsson, L., Hodges, K. I., Esch, M., Keenlyside, N., Kornblueh, L., Luo, J. J., & Yamagata, T. (2007). How may tropical cyclones change in a warmer climate? *Tellus, Series A: Dynamic Meteorology and Oceanography*, *59 A*(4), 539–561. https://doi.org/10.1111/j.1600-0870.2007.00251.x

Biswas, M. K., Stark, D., & Carson, L. (2018). *GFDL Vortex tracker users' guide V3.9a*., p. 35.

Camargo, S. J. (2013). Global and regional aspects of tropical cyclone activity in the CMIP5 models. *Journal of Climate*, *26*(24), 9880–9902. https://doi.org/10.1175/JCLI-D-12-00549.1

Camargo, S. J., Sobel, A. H., Delgenio, A. D., Jonas, J. A., Kelley, M., Lu, Y., et al. (2016). Tropical cyclones in the GISS ModelE2. *Tellus, Series A: Dynamic Meteorology and Oceanography*, *68*(1), 1–21. https://doi.org/10.3402/tellusa.v68.31494

Camargo, S. J., & Wing, A. A. (2016). Tropical cyclones in climate models. *Wiley Interdisciplinary Reviews: Climate Change*, *7*(2), 211–237. https://doi.org/10.1002/wcc.373

Caron, L. P., & Jones, C. G. (2012). Understanding and simulating the link between African easterly waves and Atlantic tropical cyclones using a regional climate model: The role of domain size and lateral boundary conditions. *Climate Dynamics*, *39*(1–2), 113–135. https://doi.org/10.1007/s00382-011-1160-8

Caron, L. P., Jones, C. G., Vaillancourt, P. A., & Winger, K. (2013). On the relationship between cloud-radiation interaction, atmospheric stability and Atlantic tropical cyclones in a variable-resolution climate model. *Climate Dynamics*, *40*(5–6), 1257–1269. https://doi.org/10.1007/s00382-012-1311-6

Caron, L. P., Jones, C. G., & Winger, K. (2011). Impact of resolution and downscaling technique in simulating recent Atlantic tropical cylone activity. *Climate Dynamics*, *37*(5), 869–892. https://doi.org/10.1007/s00382-010-0846-7

Chavas, D. R., & Emanuel, K. A. (2010). A QuikSCAT climatology of tropical cyclone size. *Geophysical Research Letters*, *37*(18), 10–13. https://doi.org/10.1029/2010GL044558

Chavas, D. R., Reed, K. A., & Knaff, J. A. (2017). Physical understanding of the tropical cyclone wind-pressure relationship. *Nature Communications*, *8*(1). https://doi.org/10.1038/s41467-017-01546-9. Retrieved from http://dx.doi.org/10.1038/s41467-017-01546-9

Cione, J. J., & Uhlhorn, E. W. (2003). Sea surface temperature variability in hurricanes: Implications with respect to intensity change. *Monthly Weather Review*, *131*(8PART 2), 1783–1796. https://doi.org/10.1175//2562.1

Daloz, A. S., Chauvin, F., & Roux, F. (2012). Impact of the configuration of stretching and ocean-atmosphere coupling on tropical cyclone activity in the variable-resolution GCM ARPEGE. *Climate Dynamics*, *39*(9–10), 2343–2359. https://doi.org/10.1007/s00382-012-1561-3

EC-Earth. (2018). *ECEarthConsortium ECEarth3PHR model output prepared for CMIP6 HighResMIP*. Retrieved from https://doi.org/10.22033/ESGF/CMIP6.2323

EC-Earth. (2019). *ECEarthConsortium ECEarth3P model output prepared for CMIP6 HighResMIP*. Retrieved from https://doi.org/10.22033/ESGF/CMIP6.2322

Elsner, J. B. (2020). Continued increases in the intensity of strong tropical cyclones. *Bulletin of the American Meteorological Society*, *101*(8), E1301–E1303. https://doi.org/10.1175/bams-d-19-0338.1

Elsner, J. B., Kossin, J. P., & Jagger, T. H. (2008). The increasing intensity of the strongest tropical cyclones. *Nature*, *455*(7209), 92–95. https://doi.org/10.1038/nature07234

Emanuel, K. (2001). Contribution of tropical cyclones to meridional heat transport by the oceans. *Journal of Geophysical Research*, *106*(D14), 14771–14781. https://doi.org/10.1029/2000JD900641

Emanuel, K. (2005). Increasing destructiveness of tropical cyclones over the past 30 years. *Nature*, *436*(7051), 686–688. https://doi.org/10.1038/nature03906

Emanuel, K. (2013). Downscaling CMIP5 climate models shows increased tropical cyclone activity over the 21st century. *Proceedings of the National Academy of Sciences of the United States of America*, *110*(30), 12219–12224. https://doi.org/10.1073/pnas.1301293110

Emanuel, K. (2020). Response of global tropical cyclone activity to increasing CO 2: Results from downscaling CMIP6 models. *Journal of Climate*, 1–54. https://doi.org/10.1175/JCLI-D-20-0367.1

Eyring, V., Bock, L., Lauer, A., Righi, M., Schlund, M., Andela, B., et al. (2019). ESMValTool v2.0 Extended set of large-scale diagnostics for quasi-operational and comprehensive evaluation of Earth system models in CMIP. *Geoscientific Model Development Discussions*, 1–81. https://doi.org/10.5194/gmd-2019-291

Goldenberg, S. B., & Shapiro, L. J. (1996). Physical mechanisms for the association of El Niño and west African rainfall with Atlantic major hurricane activity. *Journal of Climate*, *9*(6), 1169–1187. https://doi.org/10.1175/1520-0442(1996)009<1169:PMFTAO>2.0.CO;2

Gutmann, E. D., Rasmussen, R. M., Liu, C., Ikeda, K., Bruyere, C. L., Done, J. M., et al. (2018). Changes in hurricanes from a 13-Yr convection-permitting pseudo- global warming simulation. *Journal of Climate*, *31*(9), 3643–3657. https://doi.org/10.1175/JCLI-D-17-0391.1

Haarsma, R. J., Acosta, M., Bakhshi, R., Bretonnière, P.-A., Caron, L.-P., Castrillo, M., et al. (2020). HighResMIP versions of EC-Earth: EC-Earth3P and EC-Earth3P-HR description, model computational performance and basic validation. *Geoscientific Model Development*, *13*(8), 3507–3527. https://doi.org/10.5194/gmd-13-3507-2020

Haarsma, R. J., Roberts, M. J., Vidale, P. L., Catherine, A., Bellucci, A., Bao, Q., et al. (2016). High resolution model intercomparison project (HighResMIP v1.0) for CMIP6. *Geoscientific Model Development*, *9*(11), 4185–4208. https://doi.org/10.5194/gmd-9-4185-2016

Hersbach, H., Bell, B., Berrisford, P., Hirahara, S., Horányi, A., Muñoz-Sabater, J., et al. (2020). The ERA5 global reanalysis. *Quarterly Journal of the Royal Meteorological Society*, *146*(730), 1999–2049. https://doi.org/10.1002/qj.3803

Kantha, L. (2006). Time to replace the Saffir-Simpson hurricane scale? *Eos*, *87*(1), 3–6. https://doi.org/10.1029/2006eo010003

Kim, H. S., Vecchi, G. A., Knutson, T. R., Anderson, W. G., Delworth, T. L., Rosati, A., et al. (2014). Tropical cyclone simulation and response to CO2 doubling in the GFDL CM2.5 high-resolution coupled climate model. *Journal of Climate*, *27*(21), 8034–8054. https://doi.org/10.1175/JCLI-D-13-00475.1

Klotzbach, P. J., Bell, M. M., Bowen, S. G., Gibney, E. J., Knapp, K. R., & Schreck, C. J. (2020). Surface pressure a more skillful predictor of normalized hurricane damage than maximum sustained wind. *Bulletin of the American Meteorological Society*, *101*(6), E830–E846. https://doi.org/10.1175/bams-d-19-0062.1

Knapp, K. R., Diamond, H. J., Kossin, J. P., Kruk, M. J., & Schreck, C. J. I. (2018). *International best track archive for climate stewardship (IBTrACS) project, version 4*. NOAA National Centers for Environmental Information. Retrieved from https://doi.org/10.25921/82ty-9e16(26.11.2020

Knutson, T., Camargo, S. J., Chan, J. C., Emanuel, K., Ho, C. H., Kossin, J., et al. (2019). Tropical cyclones and climate change assessment. *Bulletin of the American Meteorological Society*, *100*(10), 1987–2007. https://doi.org/10.1175/BAMS-D-18-0189.1

Knutson, T., Sirutis, J. J., Zhao, M., Tuleya, R. E., Bender, M., Vecchi, G. A., et al. (2015). Global projections of intense tropical cyclone activity for the late twenty-first century from dynamical downscaling of CMIP5/RCP4.5 scenarios. *Journal of Climate*, *28*(18), 7203–7224. https://doi.org/10.1175/JCLI-D-15-0129.1

Kozar, M. E., & Misra, V. (2019). Integrated kinetic energy in north Atlantic tropical cyclones: Climatology, analysis, and seasonal applications. In *Hurricane risk* (pp. 43–69). Springer.

Landsea, C. W. (2000). *Seasonal predictability of tropical cyclones. El Nino and the southern oscillation: Multiscale variability and global and regional impacts* (pp. 149–182).

Lavender, S. L., & Walsh, K. J. (2011). Dynamically downscaled simulations of Australian region tropical cyclones in current and future climates. *Geophysical Research Letters*, *38*(10), 1–6. https://doi.org/10.1029/2011gl047499

Lee, C. Y., Tippett, M. K., Sobel, A. H., & Camargo, S. J. (2018). An environmentally forced tropical cyclone hazard model. *Journal of Advances in Modeling Earth Systems*, *10*(1), 223–241. https://doi.org/10.1002/2017MS001186

Mahendran, M. (1998). Cyclone intensity categories. *Weather and Forecasting*, *13*(3), 878–883.

Manganello, J. V., Hodges, K. I., Kinter, J. L., Cash, B. A., Marx, L., Jung, T., et al. (2012). Tropical cyclone climatology in a 10-km global atmospheric GCM: Toward weather-resolving climate modeling. *Journal of Climate*, *25*(11), 3867–3893. https://doi.org/10.1175/JCLI-D-11-00346.1

Moon, Y., Kim, D., Camargo, S. J., Wing, A. A., Sobel, A. H., Murakami, H., et al. (2020). Azimuthally averaged wind and thermodynamic structures of tropical cyclones in global climate models and their sensitivity to horizontal resolution. *Journal of Climate*, *33*(4), 1575–1595. https://doi.org/10.1175/JCLI-D-19-0172.1

National Hurricane Center. (2018). *Costliest U.S. tropical cyclones tables updated (technical report). NOAA*. Retrieved from https://www.nhc.noaa.gov/news/UpdatedCostliest.pdf

Patricola, C. M., Saravanan, R., & Chang, P. (2018). The response of atlantic tropical cyclones to suppression of African easterly waves. *Geophysical Research Letters*, *45*(1), 471–479. https://doi.org/10.1002/2017GL076081

Powell, M. D., & Reinhold, T. A. (2007). Tropical cyclone destructive potential by integrated kinetic energy. *Bulletin of the American Meteorological Society*, *88*(4), 513–526. https://doi.org/10.1175/bams-88-4-513

Ramsay, H. (2017). *The global climatology of tropical cyclones*. https://doi.org/10.1093/acrefore/9780199389407.013.79

Righi, M., Andela, B., Eyring, V., Lauer, A., Predoi, V., Schlund, M., et al. (2020). Earth System Model Evaluation Tool (ESMValTool) v2.0-technical overview. *Geoscientific Model Development*, *13*(3), 1179–1199. https://doi.org/10.5194/gmd-13-1179-2020

Roberts, M. J. (2017a). *MOHC HadGEM3GC31HM model output prepared for CMIP6 HighResMIP*. Retrieved from https://doi.org/10.22033/ESGF/CMIP6.446

Roberts, M. J. (2017b). *MOHC HadGEM3GC31MM model output prepared for CMIP6 HighResMIP*. Retrieved from https://doi.org/10.22033/ESGF/CMIP6.1902

Roberts, M. J., Baker, A., Blockley, E. W., Calvert, D., Coward, A., Hewitt, H. T., et al. (2019). Description of the resolution hierarchy of the global coupled HadGEM3-GC3.1 model as used in CMIP6 HighResMIP experiments. *Geoscientific Model Development*, *12*(12), 4999–5028. https://doi.org/10.5194/gmd-12-4999-2019

Roberts, M. J., Camp, J., Seddon, J., Vidale, P. L., Hodges, K., Vanniere, B., et al. (2020a). Impact of model resolution on tropical cyclone simulation using the HighResMIP-PRIMAVERA multimodel ensemble. *Journal of Climate*, *33*(7), 2557–2583. https://doi.org/10.1175/JCLI-D-19-0639.1

Roberts, M. J., Camp, J., Seddon, J., Vidale, P. L., Hodges, K., Vannière, B., et al. (2020b). Projected future changes in tropical cyclones using the CMIP6 HighResMIP multimodel ensemble. *Geophysical Research Letters*, *47*(14), 1–12. https://doi.org/10.1029/2020GL088662

Roberts, M. J., Vidale, P. L., Mizielinski, M. S., Demory, M. E., Schiemann, R., Strachan, J., et al. (2015). Tropical cyclones in the UPSCALE ensemble of high-resolution global climate models. *Journal of Climate*, *28*(2), 574–596. https://doi.org/10.1175/JCLI-D-14-00131.1

Roberts, M. J., Vidale, P. L., Senior, C., Hewitt, H. T., Bates, C., Berthou, S., et al. (2018). The benefits of global high resolution for climate simulation process understanding and the enabling of stakeholder decisions at the regional scale. *Bulletin of the American Meteorological Society*, *99*(11), 2341–2359. https://doi.org/10.1175/BAMS-D-15-00320.1

Simpson, R. (1971). A proposed scale for ranking hurricanes by intensity. *Minutes of the eighth NOAA, NWS hurricane conference*. Miami.

Strachan, J., Vidale, P. L., Hodges, K., Roberts, M., & Demory, M. E. (2013). Investigating global tropical cyclone activity with a hierarchy of AGCMs: The role of model resolution. *Journal of Climate*, *26*(1), 133–152. https://doi.org/10.1175/JCLI-D-12-00012.1

Vannière, B., Roberts, M., Vidale, P. L., Hodges, K., Demory, M.-E., Caron, L.-P., et al. (2020). The moisture budget of tropical cyclones in HighResMIP models: Large-scale environmental balance and sensitivity to horizontal resolution. *Journal of Climate*, *33*(9), 1–51. https://doi.org/10.1175/jcli-d-19-0999.1

Voldoire, A. (2019a). *CNRMCERFACS CNRMCM61 model output prepared for CMIP6 HighResMIP*. Retrieved from https://doi.org/10.22033/ESGF/CMIP6.1925

Voldoire, A. (2019b). *CNRMCERFACS CNRMCM61HR model output prepared for CMIP6 HighResMIP*. Retrieved from https://doi.org/10.22033/ESGF/CMIP6.1387

Voldoire, A., Saint-Martin, D., Sénési, S., Decharme, B., Alias, A., Chevallier, M., et al. (2019). Evaluation of CMIP6 DECK experiments with CNRM-CM6-1. *Journal of Advances in Modeling Earth Systems*, *11*(7), 2177–2213. https://doi.org/10.1029/2019MS001683

Walsh, K. J., Fiorino, M., Landsea, C. W., & McInnes, K. L. (2007). Objectively determined resolution-dependent threshold criteria for the detection of tropical cyclones in climate models and reanalyzes. *Journal of Climate*, *20*(10), 2307–2314. https://doi.org/10.1175/JCLI4074.1

Wang, S., & Toumi, R. (2016). On the relationship between hurricane cost and the integrated wind profile. *Environmental Research Letters*, *11*(11). https://doi.org/10.1088/1748-9326/11/11/114005

Wang, S., & Toumi, R. (2018a). A historical analysis of the mature stage of tropical cyclones. *International Journal of Climatology*, *38*(5), 2490–2505. https://doi.org/10.1002/joc.5374

Wang, S., & Toumi, R. (2018b). Reduced sensitivity of tropical cyclone intensity and size to sea surface temperature in a radiative-convective equilibrium environment. *Advances in Atmospheric Sciences*, *35*(8), 981–993. https://doi.org/10.1007/s00376-018-7277-5

Wehner, M., Prabhat, Reed, K. A., Stone, D., Collins, W. D., & Bacmeister, J. (2015). Resolution dependence of future tropical cyclone projections of CAM5.1 in the U.S. CLIVAR hurricane working group idealized configurations. *Journal of Climate*, *28*(10), 3905–3925. https://doi.org/10.1175/jcli-d-14-00311.1

Yamada, Y., Satoh, M., Sugi, M., Kodama, C., Noda, A. T., Nakano, M., & Nasuno, T. (2017). Response of tropical cyclone activity and structure to global warming in a high-resolution global nonhydrostatic model. *Journal of Climate*, *30*(23), 9703–9724. https://doi.org/10.1175/JCLI-D-17-0068.1

Zarzycki, C. M., & Jablonowski, C. (2014). A multidecadal simulation of Atlantic tropical cyclones using a variable-resolution global atmospheric general circulation model. *Journal of Advances in Modeling Earth Systems*, *6*(3), 805–828. https://doi.org/10.1002/2013MS000282. Received

Zhai, A. R., & Jiang, J. H. (2014). Dependence of US hurricane economic loss on maximum wind speed and storm size. *Environmental Research Letters*, *9*(6). https://doi.org/10.1088/1748-9326/9/6/064019